Front. Mater. Sci. 2023, 17(3): 230653
https://doi.org/10.1007/s11706-023-0653-9

RESEARCH ARTICLE

Polyurethane foam-supported three-dimensional interconnected graphene nanosheets network encapsulated in polydimethylsiloxane to achieve significant thermal conductivity enhancement

Wenjing Li*, Ni Wu*, Sai Che, Li Sun, Hongchen Liu, Guang Ma, Ye Wang, Chong Xu, and Yongfeng Li (✉)

State Key Laboratory of Heavy Oil Processing, China University of Petroleum, Beijing 102249, China

ABSTRACT: **Polyurethane (PU) foams are widely used in thermal management materials due to their good flexibility. However, their low thermal conductivity limits the efficiency. To address this issue, we developed a new method to produce tannic acid (TA)-modified graphene nanosheets (GTs)-encapsulated PU (PU@GT) foams using the soft template microstructure and a facile layer-by-layer (L-B-L) assembly method. The resulting PU@GT scaffolds have ordered and tightly stacked GTs layers that act as three-dimensional (3D) highly interconnected thermal networks. These networks are further infiltrated with polydimethylsiloxane (PDMS). The through-plane thermal conductivity of the polymer composite reaches 1.58 $W \cdot m^{-1} \cdot K^{-1}$ at a low filler loading of 7.9 wt.%, which is 1115% higher than that of the polymer matrix. Moreover, the mechanical property of the composite is ~2 times higher than that of the polymer matrix while preserving good flexibility of the polymer matrix owing to the retention of the PU foam template and the construction of a stable 3D graphene network. This work presents a facile and scalable production approach to fabricate lightweight PU@GT/PDMS polymer composites with excellent thermal and mechanical performance, which implies a promising future in thermal management systems of electronic devices.**

KEYWORDS: **graphene nanosheet; polyurethane foam; polymer composite; thermal and mechanical property**

Contents

Received April 2, 2023; accepted June 7, 2023

E-mail: yfli@cup.edu.cn

∗ W.L. and N.W. contributed equally to this study.

1 Introduction

Thermal management systems are becoming increasingly important with the development of miniaturization and integration of electronic devices. The intensive packaging of integrated circuits and electronic components releases significant amounts of heat that affects the performance and lifetime of microelectronic devices. Therefore, developing high-performance thermal management materials to enhance the heat transfer capability of electronic devices has become a research focus [1].

Polymeric materials are widely used in electrical equipment and electronic devices due to their easy processing, light weight, high toughness, and low price [2]. However, the majority of polymeric materials possess low thermal conductivity due to the severe phonon scattering caused by the free orientation and random entanglement of polymer molecular chain segments [3]. To improve the thermal conductivity of polymeric materials, researchers have introduced high-performance thermally conductive fillers that allow more heat to be transferred along the pathways made up of thermally conductive fillers [4]. Graphene is a two-dimensional (2D) material composed of sp^2 hybridized carbon atoms that has a high intrinsic thermal conductivity of up to ~5300 $W \cdot m^{-1} \cdot K^{-1}$. This is several orders of magnitude higher than that of conventional thermal conductive materials such as copper and aluminum [5]. Graphene is lightweight, flexible, and chemically stable, making it a promising material for thermal management applications. However, the application of graphene is limited by the difficulty of dispersion in polymers and insufficient thermal pathways. To address these challenges, researchers have made various efforts to build three-dimensional (3D) continuous filler networks [6–9]. The 3D graphene networks promote effective heat conduction throughout the composite material with minimal filler loading by providing continuous heat transfer paths to reduce the interfacial thermal resistance between the filler and the polymer substrate [10]. Several technologies have been developed to fabricate 3D graphene networks in polymers, such as chemical vapor deposition [11–12], ice-template method [13–14], and hydrothermal method [15–16]. However, these approaches often require complex and demanding preparation processes. Therefore, the resulting materials have limited scalability and reproducibility.

The polymer foam template assembly method is a simple and promising approach to create 3D interconnected filler networks within a polymer matrix [6,17–18]. For example, Han et al. prepared graphene foams (GFs) by the assembly method of graphene nanosheets (GTs) on melamine resin foam backbone [19]. The resulting polydimethylsiloxane (PDMS) composite showed a high thermal conductivity of 0.22 $W \cdot m^{-1} \cdot K^{-1}$ at an ultra-low GF loading of 0.7 wt.%. Wang et al. constructed 3D boron nitride nanosheet-coated melamine foam (MF@BNNS) by layer-by-layer (L-B-L) assembly on MF templates [20], and the prepared epoxy (EP)/MF@BNNS composite achieved a high thermal conductivity of 0.6 $W \cdot m^{-1} \cdot K^{-1}$ at a loading of ~1.1 vol.%. These applications demonstrate the potential of the soft polymer foam template approach for the preparation of thermally conductive composites. However, the challenge lies in how to further enhance the tight integration of the filler with the foam template to appropriately increase the filler loading and simultaneously enhance the thermally conductive and mechanical properties of the composites.

In this study, we propose a simple and scalable approach to fabricate high-performance thermal management materials by encapsulating a 3D interconnected GTs network within the PDMS matrix supported by the polyurethane (PU) foam. The hydrophilic GTs are first obtained as building blocks using the tannic acid (TA)-assisted ball milling technique. The 3D PU foam-supported GT networks (PU@GT) are fabricated by repetitive L-B-L assembly of anionic GTs and cationic histidine (His) on commercial PU foams driven by electrostatic interactions. The 3D PU@GT foam is further encapsulated with PDMS to obtain the composites (PU@GT/PDMS). The thermal conductivities of the corresponding PDMS composites manufactured under different L-B-L deposition times are investigated. As a result, the PU@GT/PDMS composite achieves a high thermal conductivity of 1.58 $W \cdot m^{-1} \cdot K^{-1}$ at a relatively low filler loading of 7.9 wt.%, which is enhanced by 1115% and 129% compared with pure PDMS and GT/PDMS prepared by the conventional co-blending method, respectively. In addition, the PU@GT/PDMS

composite also exhibits significantly improved tensile strength and flexibility thanks to the PU foam as a soft template and the constructed 3D filler network. Therefore, the developed composite material holds great potential for thermal management applications.

2 Experimental

2.1 Materials

Graphene powder (G) was purchased from Jiangsu Guoshi New Energy Technology Co., Ltd. TA was obtained from Shanghai Maclin Biochemical Technology Co., Ltd. PU foam was provided from Top Group Daily Chemicals Co., Ltd. His was offered by Shanghai Aladdin Reagent Co., Ltd. PDMS and the curing agent were supplied from Dow Chemical Co., Ltd. The average molecular weight of PDMS is ~16 000, and the curing agent contains: siloxanes and silicones, di-Me, Me hydrogen; dimethyl siloxane, dimethylsiloxy-terminated; dimethylvinylated and trimethylated silica. All chemicals were used as received without further purification.

2.2 Preparation of GTs

In this work, functionalized GTs were obtained by the TA-assisted ball milling method according to our previous work [21]. Briefly, 2 g of graphene powder (~5 μm) was added into a solution of TA (40 mg·mL^{-1}) under stirring and ultrasonication. The mixture was then poured into stainless steel jars for ball milling for 9 h. The resulting mixture was centrifuged to collect the supernatant, and then vacuum filtered, washed with deionized water, and dried to obtain TA-modified GTs.

2.3 Preparation of PU@GT

PU@GT was prepared by the L-B-L self-assembly method to coat GTs onto the PU skeleton via the electrostatic interactions of positively charged PU and negatively charged GT. First, the PU foam was completely immersed in the histidine solution (5 mg·mL^{-1}) for 3 min. After squeezing out the excess liquid, the foam was placed in the oven to completely remove the water, and then immersed the GT dispersion for 3 min. Next, the foam was taken out and dried, followed by immersion in the His solution. Finally, the above operation was repeated in cycles. x is the number of deposition cycles, and the resulting foam was noted as PU@GT-x (x = 5, 10, 15, 20, 25).

2.4 Preparation of PU@GT/PDMS composites

PDMS and its curing agent are mixed in a mass ratio of 10:1. Then, the PU@GT-x foam was put into the mold and the PDMS mixture was added for vacuum impregnation. Finally, the mold was placed in an oven and heated at 80 °C for 4 h to obtain the PU@GT-x/PDMS composites. For comparison, GT/PDMS composites with random distribution of fillers were also prepared by the direct blending method under the same curing conditions, i.e., without using the PU foam.

2.5 Characterization

The morphology and microstructure of the samples were characterized using scanning electron microscopy (SEM; Hitachi SU3500). The chemical structures of the samples were studied by Fourier transform infrared spectroscopy (FTIR; Bruker Tensor II spectrometer). The thermal stability of the sample was measured by the thermogravimetric analysis (TGA; STA7200) from 30 to 800 °C in N_2 atmosphere. The zeta potentials of samples were measured under the nanoparticle size and zeta potential analyzer (Zetasizer Nano ZS). The contact angle data were characterized by the optical contact angle & interface tension meter (KINO SL200KS). The cross-plane thermal conductivities of PDMS composites were collected on the LW-9389 TIM Tester (Longwin, Taiwan, China) using the steady-state heat flow. The mechanical property of the samples was recorded on a universal testing machine (Zwick Roell Z010), and the specific tensile testing methodology was referenced to the ASTM D412 standard. The geometry of the specimen used for tensile testing was a C-shaped dumbbell (ASTM D412 Type C) with an overall length of 115 mm (4.5 in.), a scale length of 25 mm (1 in.), a measured width of 6 mm (0.25 in.), and a thickness of 3 mm.

3 Results and discussion

3.1 Structural characterization of PU@GT/PDMS composites

The fabrication process of PU@GT/PDMS composites is shown in Fig. 1. Briefly, anionic GT and cationic His

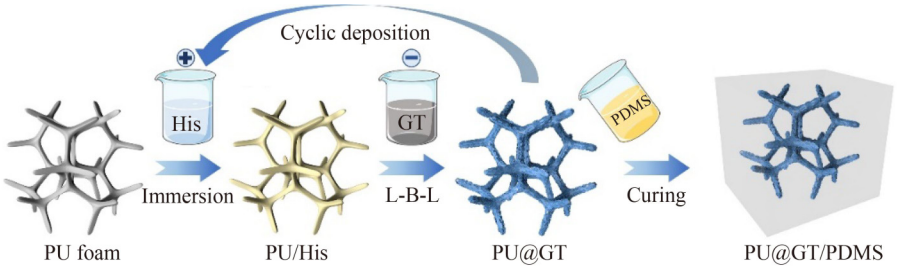

Fig. 1 Schematic diagram of the preparation for PU@GT/PDMS.

were alternately deposited on the PU backbone surface by the L-B-L assembly technique, and then the composites were obtained by the encapsulation with PDMS. Considering the poor dispersion of graphene flakes in the aqueous solution, graphene flakes were first treated by surface modification through the TA solution-assisted ball milling technique.

As displayed in Fig. 2(a), pristine graphene flakes with an average lateral size of about 5 μm are observed. After ball milling, the average lateral size of modified GTs is reduced to ~3 μm and the hydrophilicity is dramatically improved with the change of the water contact angle from 78° to 30° (Fig. 2(b)). The resulting GTs exhibit a homogeneous dispersion state in water showing an obvious Tyndall effect (Fig. 2(d)) owing to the presence of abundant hydrophilic hydroxyl groups in the TA structure, which is conducive to the subsequent L-B-L assembly process. In addition, the successful surface modification of GTs is further demonstrated by FTIR and TGA (Figs. S1 and S2).

His is positively charged in water due to the presence of amino groups. The TA modification introduces hydroxyl functional groups on the surface of GTs, and GTs are negatively charged in water. Therefore, His and GT are here used as cationic and anionic adsorbents, respectively, and coated alternately on the PU backbone by the L-B-L assembly technique. To verify the feasibility, the zeta potentials of His and GT in the aqueous solution were measured. As shown in Fig. 2(c), the zeta potential of the His solution is about 35 mV, while that of the GT aqueous dispersion is about −38 mV, indicating the existence of the electrostatic interaction between His and GT. Figure 2(d) displays optical photographs of GT and GT/His suspensions. After the addition of His into the GT dispersion (right), the dispersion of the GT suspension deteriorated and began to form large aggregates settling at the bottle bottom due to the strong electrostatic interaction between His and GTs, leading to the appearance of the

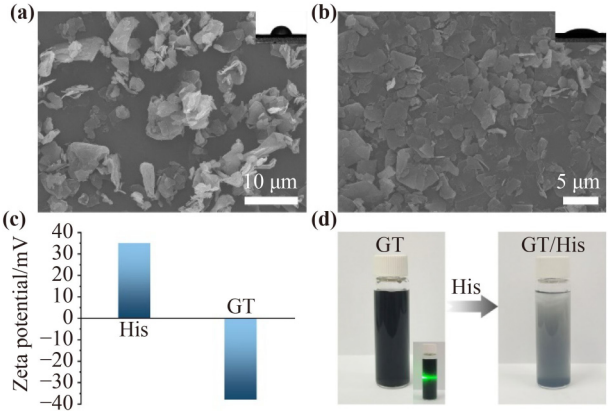

Fig. 2 SEM images of (**a**) pristine graphene nanosheets and (**b**) GT. (**c**) Zeta potentials of GT and His aqueous solutions. (**d**) Optical photos of GT dispersions before (left) and after (right) the addition of His.

obvious stratification phenomenon. The above results further suggest the presence of the electrostatic interaction between His and GTs.

The PU@GT foams were achieved by the L-B-L alternate adsorption of cationic His and anionic GTs on the PU backbone, and the microstructure and the morphology are shown in Fig. 3. The pure PU foam surface is smooth, featuring an open 3D interconnected macropore structure (Fig. 3(a)). After the L-B-L self-assembly process, the surface of PU becomes rough. The GTs are tightly coated on the PU surface by strong electrostatic interactions without changing the original structure of the foam. As clearly seen in Figs. 3(b)–3(f), the number of GTs on the PU skeleton increases greatly as the deposition cycle number gradually rises from 5 to 25. This can be attributed to the fact that the addition of His in each cycle allows more GTs from the dispersion to be adsorbed on the PU backbone by the electrostatic attraction. Meanwhile, the presence of His also contributes to promoting the tight stacking of GTs, which facilitates the formation of continuous and complete heat transfer paths. When the deposition cycle number reaches

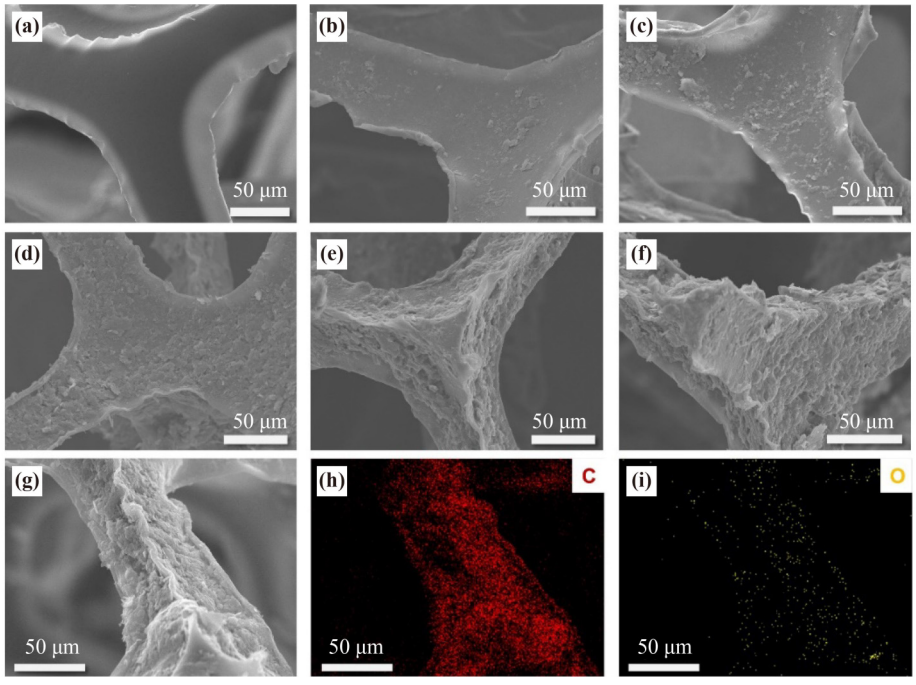

Fig. 3 Cross-sectional SEM images of (**a**) the PU foam and (**b**)(**c**)(**d**)(**e**)(**f**) PU@GT-*x* (*x* = 5, 10, 15, 20, and 25 from panel (b) to panel (f)). (**g**)(**h**)(**i**) Element mapping images of PU@GT.

15, the GTs contact each other along the PU backbone, forming a continuous thermal pathway in PU@GT-15. Moreover, a denser and more perfect graphene network is developed on the skeleton surface of PU@GT-20 and PU@GT-25. It is worth mentioning that the interaction between GTs and His eliminates the air gap and ensures a tight connection between GTs, which is beneficial to reduce the interfacial thermal resistance and improve the thermal conductivity of the composites. In addition, the element mapping images (Figs. 3(g)–3(i)) further prove that the GTs are uniformly and continuously wrapped around the PU foam backbone. After filling with PDMS, the 3D interconnect network is well maintained throughout the PDMS matrix without obvious interfacial separation (Fig. S3).

The TGA curves of PU, His, and PU@GT are presented in Fig. 4(a). Combined with Fig. S1, it can be seen that PU, His, and TA all decompose gradually with the increasing temperature under nitrogen atmosphere, while the graphene maintains excellent thermal stability without any weight loss. The graphene coating makes the thermal stability of the PU foam improve with more residual mass at high temperature, which also verifies the successful attachment of graphene to the PU backbone. The FTIR spectra of PU and PU@GT are given in Fig. 4(b), in which the characteristic peaks at 3447, 2920, and 1093 cm^{-1} of PU belong to N−H, C−H, and C−N stretching vibrations, respectively [22–24]. For PU@GT, besides the characteristic peaks of pure PU, the O−H (N−H) broadband at 3450 cm^{-1} [25–26], the C−O stretching vibration at 1352 cm^{-1} [27], and the C=C stretching vibration at 1634 cm^{-1} appear [28], which are assigned to His, TA, and graphene, respectively. The above results further indicate that the GTs are successfully bonded on the PU backbone by the L-B-L assembly method.

3.2 Thermal conductivity of PU@GT/PDMS composites

The thermal conductivity of PU@GT/PDMS composites was tested by the steady-state heat flow method. The thermal conductivity of GT/PDMS composites with randomly distributed fillers was also measured for comparison. As shown in Figs. 5(a) and 5(b), the thermal conductivity and the corresponding thermal conductivity enhancement of PU@GT/PDMS grow with the accumulation of the deposition cycle number. PU@GT-10/PDMS exhibits a limited increased thermal conductivity of 0.68 $W \cdot m^{-1} \cdot K^{-1}$ due to the extremely low filler loading. After 15 cycles, the thermal conductivity of PU@GT-15/PDMS reaches 1.27 $W \cdot m^{-1} \cdot K^{-1}$, an improvement of 87% compared to that for the 10th cycle,

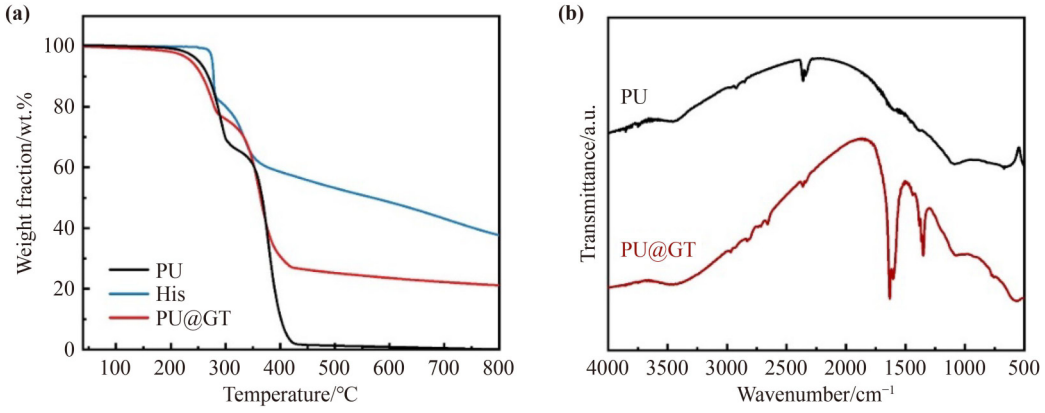

Fig. 4 (**a**) TGA curves of PU, His, and PU@GT. (**b**) FTIR spectra of PU and PU@GT.

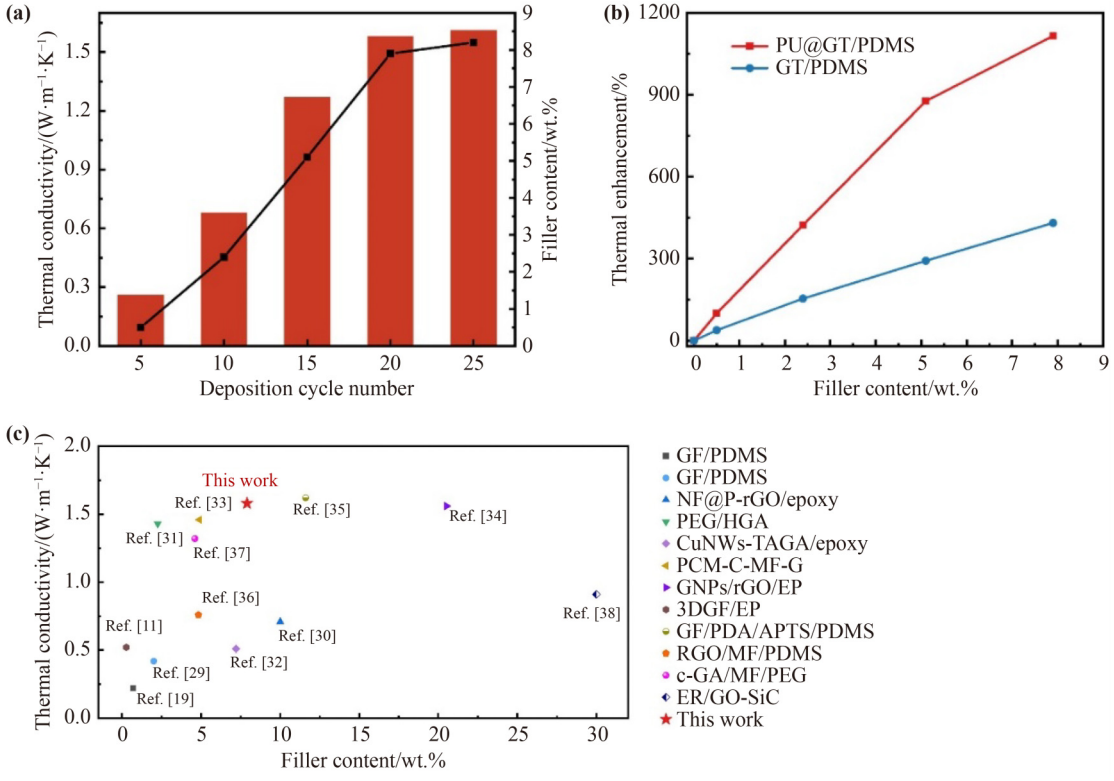

Fig. 5 (**a**) The cross-plane thermal conductivity and (**b**) the thermal conductivity enhancement of PDMS composites. (**c**) Comparison of thermal conductivities for the reported 3D graphene/polymer composites.

which can be attributed to the excellent thermal properties of GTs and the formation of a highly interconnected 3D graphene network. The GTs have high intrinsic thermal conductivity, while the 3D interconnected graphene network supported by the PU foam extends phonon transport channels and ensures the efficient heat transfer through the composite. When the deposition cycle number further increases, the thermal conductivity of PU@GT-20/PDMS rises to 1.58 $W \cdot m^{-1} \cdot K^{-1}$, corresponding to a thermal conductivity enhancement of 1115% compared to that of pure PDMS (0.13 $W \cdot m^{-1} \cdot K^{-1}$). It is noteworthy that the improvement from the 15th to the 20th deposition is not remarkable in comparison to that from the 10th to the 15th deposition, presumably as the thermal percolation threshold of the composite has been reached [20]. Subsequently, the PU@GT-25/PDMS composite reveals only a slight increase in thermal conductivity (1.61 $W \cdot m^{-1} \cdot K^{-1}$), which further confirms the above conjecture. For GT/PDMS composites with randomly distributed fillers, a quite slow thermal conductivity

enhancement trend is presented in Fig. 5(b), owning to the lack of 3D continuous thermal networks within the PDMS composite. At the same filler loading of 7.9 wt.%, the thermal conductivity enhancement of GT/PDMS is only 431%, even less than one-half of that of PU@GT-20/PDMS. These results demonstrate the huge advantage of 3D thermal networks for promoting the thermal conductivity of the polymer composite at a low filler content. Additionally, Fig. 5(c) lists cross-plane thermal conductivity values of some previously reported 3D graphene-based polymer composites [11,19,29–38]. In comparison, the present work achieves superior thermal conductivity of polymer composites at a relatively low filler loading. Compared with other methods in preparing 3D interconnected structures, the utilization of soft templates is more convenient and efficient, which has the advantage of commercial production.

3.3 Mechanical performance of PU@GT/PDMS composites

In addition to thermal conductivity, mechanical properties are also important parameters in the practical application of thermal management materials. The axial tensile tests were performed on PDMS composites, and the stress–strain curves, tensile stress, as well as elastic moduli of pure PDMS, GT/PDMS, and PU@GT-20/PDMS are displayed in Figs. 6(a) and 6(b).

The tensile stress of PU@GT/PDMS is up to 512.3 kPa, which is 1.95 times higher than that of pure PDMS (262.8 kPa) and 1.34 times higher than that of GT/PDMS. Compared with that of pure PDMS (1.3 MPa), the elastic moduli of GT/PDMS (2.8 MPa) and PU@GT/PDMS (4.0 MPa) increase by 115% and 208%, respectively. The incorporation of GTs leads to a significant improvement of the mechanical properties of PDMS, which is ascribed to the inherent excellent mechanical strength of graphene. In addition, the PU foam provides a strong support for the 3D graphene network, thus the retention of the PU foam template and the continuous graphene network play a positive role in further strengthening the mechanical properties of PU@GT/PDMS composites. Moreover, the flexibility of the PU foam gives PU@GT/PDMS a better elastic deformation ability, which prolongs its breakpoint deformation from 24.3% to 36.0%. However, as for GT/PDMS, the addition of fillers results in an elevated tensile strength at the expense of the flexibility due to the lack of the PU template support.

Figure 6(c) depicts optical photos of PU@GT before and after the compression. The presence of the PU foam imparts excellent compressibility to PU@GT and there is no filler shedding after 50 compressions (Fig. S4). This is because the addition of His facilitates the binding of PU to GT and the tight stacking between GTs through electrostatic interactions, thus preventing the nanosheets from falling off the PU foam surface.

In short, the L-B-L self-assembly strategy based on the PU foam not only significantly improves the thermal

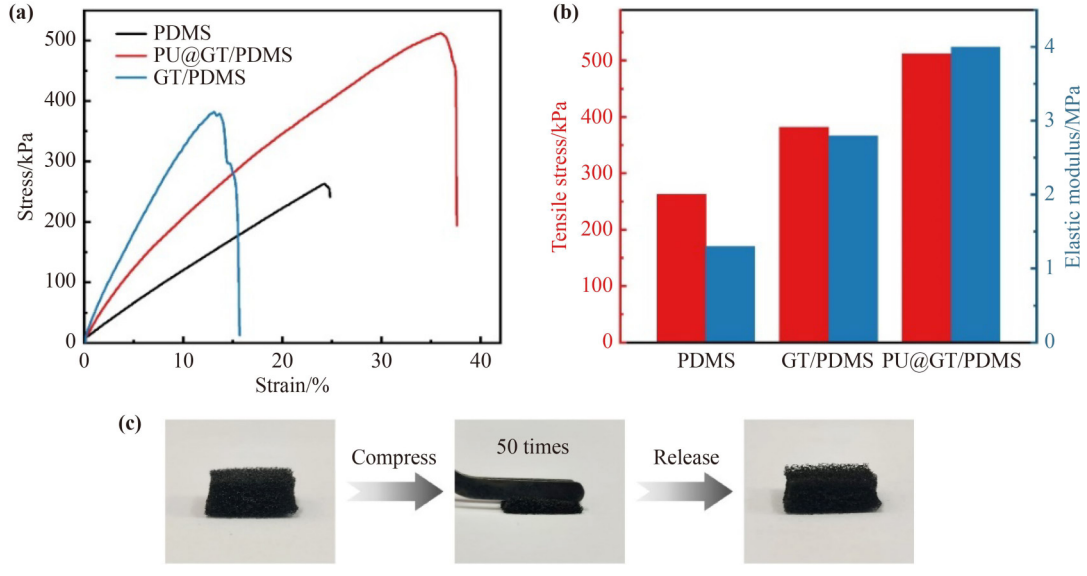

Fig. 6 (**a**) Tensile stress–strain curves and (**b**) tensile stress/elastic modulus values of PDMS and the PDMS composites. (**c**) Optical photos of PU@GT after 50 compressions.

conductivity of PDMS composites at a low filler content, but also reinforces the mechanical strength and flexibility of the polymer composites.

4 Conclusions

In conclusion, we have demonstrated a facile and scalable approach to achieve significant thermal conductivity enhancement by encapsulating a 3D interconnected GTs network within a PDMS matrix supported by the PU foam. At a low filling content of 7.9 wt.%, the resulting composite material exhibits a high thermal conductivity of 1.58 $W \cdot m^{-1} \cdot K^{-1}$, which is 11 times higher than that of the pure PDMS matrix. The high thermal conductivity of the composite material can be attributed to the formation of a highly interconnected 3D graphene network within the PDMS matrix, which facilitates the efficient heat transfer across the composite material. The lightweight porous structure of the PU foam also plays a key role in improving the overall performance of the composites by providing structural support for the construction of the 3D GT thermal network and giving the composites superior compressibility, tensile strength, and flexibility. Overall, the developed PU@GT/PDMS composite holds great promise for a wide range of thermal management applications.

Disclosure of potential conflicts of interests The authors declare that they have no known competing financial interests or personal relationships that could have appeared to influence the work reported in this paper.

Acknowledgements We gratefully acknowledge the financial supports from the National Natural Science Foundation of China (Grant Nos. 22238012, 22178384, 21908245, and 52002363) and the Science Foundation of China University of Petroleum, Beijing (Grant No. ZX20220079).

Electronic supplementary information Supplementary materials can be found in the online version at https://doi.org/10.1007/s11706-023-0653-9, which include Figs. S1–S4.

References

[1] Guo X X, Cheng S J, Cai W W, et al. A review of carbon-based thermal interface materials: Mechanism, thermal measurements and thermal properties. Materials & Design, 2021, 209: 109936

[2] Feng L, Wang W, Song B, et al. Synthesis of P, N and Si-containing waterborne polyurethane with excellent flame retardant, alkali resistance and flexibility via one-step synthetic approach. Progress in Organic Coatings, 2023, 174: 107286

[3] He X H, Wang Y C. Recent advances in the rational design of thermal conductive polymer composites. Industrial & Engineering Chemistry Research, 2021, 60(3): 1137–1154

[4] Zhu X L, Li Q Y, Wang L, et al. Current advances of polyurethane/graphene composites and its prospects in synthetic leather: a review. European Polymer Journal, 2021, 161: 110837

[5] Huang X Y, Zhi C Y, Lin Y, et al. Thermal conductivity of graphene-based polymer nanocomposites. Materials Science and Engineering R: Reports, 2020, 142: 100577

[6] Wu N, Che S, Li W H, et al. A review of three-dimensional graphene networks for use in thermally conductive polymer composites: construction and applications. New Carbon Materials, 2021, 36(5): 911–926

[7] de Luna M S, Wang Y, Zhai T, et al. Nanocomposite polymeric materials with 3D graphene-based architectures: from design strategies to tailored properties and potential applications. Progress in Polymer Science, 2019, 89: 213–249

[8] Zhan H F, Nie Y H, Chen Y, et al. Thermal transport in 3D nanostructures. Advanced Functional Materials, 2020, 30(8): 1903841

[9] Kim J E, Oh J H, Kotal M, et al. Self-assembly and morphological control of three-dimensional macroporous architectures built of two-dimensional materials. Nano Today, 2017, 14: 100–123

[10] Zhang F, Feng Y Y, Feng W. Three-dimensional interconnected networks for thermally conductive polymer composites: design, preparation, properties, and mechanisms. Materials Science and Engineering R: Reports, 2020, 142: 100580

[11] Zhou H Z, Wang H J, Du X S, et al. Facile fabrication of large 3D graphene filler modified epoxy composites with improved thermal conduction and tribological performance. Carbon, 2018, 139: 1168–1177

[12] Wu Z, Xu C, Ma C, et al. Synergistic effect of aligned graphene nanosheets in graphene foam for high-performance thermally conductive composites. Advanced Materials, 2019, 31(19): 1900199

[13] Min P, Liu J, Li X F, et al. Thermally conductive phase change composites featuring anisotropic graphene aerogels for real-time and fast-charging solar-thermal energy conversion. Advanced Functional Materials, 2018, 28(51): 1805365

[14] Yao Y, Sun J, Zeng X, et al. Construction of 3D skeleton for polymer composites achieving a high thermal conductivity. Small, 2018, 14(13): 1704044

[15] Zhang W, Kong Q Q, Tao Z, et al. 3D thermally cross-linked graphene aerogel-enhanced silicone rubber elastomer as thermal interface material. Advanced Materials Interfaces, 2019, 6(12): 1900147

[16] Shao L B, Shi L L, Li X H, et al. Synergistic effect of BN and graphene nanosheets in 3D framework on the enhancement of thermal conductive properties of polymeric composites. Composites Science and Technology, 2016, 135: 83–91

[17] Liu Z, Chen Y, Li Y, et al. Graphene foam-embedded epoxy composites with significant thermal conductivity enhancement. Nanoscale, 2019, 11(38): 17600–17606

[18] Dai W, Lv L, Ma T, et al. Multiscale structural modulation of anisotropic graphene framework for polymer composites achieving highly efficient thermal energy management. Advanced Science, 2021, 8(7): 2003734

[19] Han B, Chen H Y, Hu T, et al. High electrical conductivity in polydimethylsiloxane composite with tailored graphene foam architecture. Journal of Molecular Structure, 2020, 1203: 127416

[20] Wang X W, Wu P Y. Melamine foam-supported 3D interconnected boron nitride nanosheets network encapsulated in epoxy to achieve significant thermal conductivity enhancement at an ultralow filler loading. Chemical Engineering Journal, 2018, 348: 723–731

[21] Wu N, Yang W, Che S, et al. Green preparation of high-yield and large-size hydrophilic boron nitride nanosheets by tannic acid-assisted aqueous ball milling for thermal management. Composites Part A: Applied Science and Manufacturing, 2023, 164: 107266

[22] Lustriane C, Dwivany F M, Suendo V, et al. Effect of chitosan and chitosan-nanoparticles on post harvest quality of banana fruits. Journal of Plant Biotechnology, 2018, 45(1): 36–44

[23] Liu H H, Zhang L, Zuo Y, et al. Preparation and characterization of aliphatic polyurethane and hydroxyapatite composite scaffold. Journal of Applied Polymer Science, 2009, 112(5): 2968–2975

[24] Lu R, Gan W, Wu B H, et al. C−H stretching vibrations of methyl, methylene and methine groups at the vapor/alcohol (N = 1–8) interfaces. The Journal of Physical Chemistry B, 2005, 109(29): 14118–14129

[25] Lee T H, Yen C T, Hsu S H. Preparation of polyurethane–graphene nanocomposite and evaluation of neurovascular regeneration. ACS Biomaterials Science & Engineering, 2020, 6(1): 597–609

[26] Norouzi O, Mazhkoo S, Haddadi S A, et al. Hydrothermal liquefaction of green macroalgae *Cladophora glomerata*: effect of functional groups on the catalytic performance of graphene oxide/polyurethane composite. Catalysis Today, 2022, 404: 93–104

[27] Liu J, Zhang Q H, Ma F, et al. Three-step identification of infrared spectra of similar tree species to *Pterocarpus santalinus* covered with beeswax. Journal of Molecular Structure, 2020, 1218: 128484

[28] Peng H L, Wang S P, Kim M J, et al. Highly reversible electrochemical reaction of insoluble 3D nanoporous polyquinoneimines with stable cycle and rate performance. Energy Storage Materials, 2020, 25: 313–323

[29] Zhang Y, Yang F, Yu C, et al. Improved thermal properties of three-dimensional graphene network filled polymer composites. Journal of Electronic Materials, 2022, 51(1): 420–425

[30] Huang L, Zhu P L, Li G, et al. Improved wetting behavior and thermal conductivity of the three-dimensional nickel foam/epoxy composites with graphene oxide as interfacial modifier. Applied Physics A: Materials Science & Processing, 2016, 122(5): 515

[31] Yang J, Qi G Q, Liu Y, et al. Hybrid graphene aerogels/phase change material composites: thermal conductivity, shape-stabilization and light-to-thermal energy storage. Carbon, 2016, 100: 693–702

[32] Yang X T, Fan S G, Li Y, et al. Synchronously improved electromagnetic interference shielding and thermal conductivity for epoxy nanocomposites by constructing 3D copper nanowires/ thermally annealed graphene aerogel framework. Composites Part A: Applied Science and Manufacturing, 2020, 128: 105670

[33] Xue F, Lu Y, Qi X D, et al. Melamine foam-templated graphene nanoplatelet framework toward phase change materials with multiple energy conversion abilities. Chemical Engineering Journal, 2019, 365: 20–29

[34] Liang C B, Qiu H, Han Y Y, et al. Superior electromagnetic interference shielding 3D graphene nanoplatelets/reduced graphene oxide foam/epoxy nanocomposites with high thermal conductivity. Journal of Materials Chemistry C: Materials for Optical and Electronic Devices, 2019, 7(9): 2725–2733

[35] Fang H, Zhao Y, Zhang Y, et al. Three-dimensional graphene foam-filled elastomer composites with high thermal and mechanical properties. ACS Applied Materials & Interfaces, 2017, 9(31): 26447–26459

[36] Qin M M, Xu Y X, Cao R, et al. Efficiently controlling the 3D thermal conductivity of a polymer nanocomposite via a hyperelastic double-continuous network of graphene and sponge. Advanced Functional Materials, 2018, 28(45): 1805053

[37] Liao H H, Chen W H, Liu Y, et al. A phase change material encapsulated in a mechanically strong graphene aerogel with high thermal conductivity and excellent shape stability. Composites Science and Technology, 2020, 189: 108010

[38] He J, Wang H, Qu Q Q, et al. Self-assembled three-dimensional structure with optimal ratio of GO and SiC particles effectively improving the thermal conductivity and reliability of epoxy composites. Composites Communications, 2020, 22: 100448